Hydrophobic Interactions Modulate Self-Assembly of Nanoparticles

Ana Sánchez-Iglesias,[†,‡] Marek Grzelczak,[†,‡,§,*] Thomas Altantzis,[⊥] Bart Goris,[⊥] Jorge Pérez-Juste,[‡] Sara Bals,[⊥] Gustaaf Van Tendeloo,[⊥] Stephen H. Donaldson, Jr.,[¶] Bradley F. Chmelka,[¶] Jacob N. Israelachvili,[¶] and Luis M. Liz-Marzán[†,‡,§,*]

[†]Bionanoplasmonics Laboratory, CIC biomaGUNE, Paseo de Miramón 182, 20009 Donostia, San Sebastián, Spain, [‡]Departamento de Química Física, Universidade de Vigo, 36310 Vigo, Spain, [§]Ikerbasque, Basque Foundation for Science, 48011 Bilbao, Spain, [⊥]EMAT, University of Antwerp, Groenenborgerlaan 171, B-2020 Antwerp, Belgium, and [¶]Department of Chemical Engineering, University of California, Santa Barbara, California 93106, United States

ABSTRACT Hydrophobic interactions constitute one of the most important types of nonspecific interactions in biological systems, which emerge when water molecules rearrange as two hydrophobic species come close to each other. The prediction of hydrophobic interactions at the level of nanoparticles (Brownian objects) remains challenging because of uncontrolled diffusive motion of the particles. We describe here a general methodology for solvent-induced, reversible self-assembly of gold nanoparticles into 3D clusters with well-controlled sizes. A theoretical description of the process confirmed that hydrophobic interactions are the main driving force behind nanoparticle aggregation.

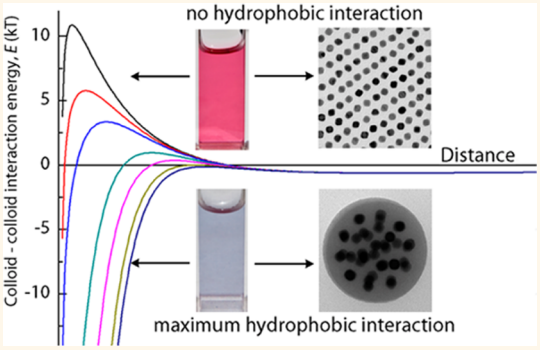

KEYWORDS: hydrophobic interactions · self-assembly · nanoparticle clusters · gold nanoparticles

The bottom-up approach to nanofabrication requires a precise organization of nanosized building blocks in three dimensions, from atomic and molecular to colloidal and microscopic length scales. Each level is dominated by different kinds of interactions that require specific tools to control the spatial distribution of the respective building blocks. At molecular and colloidal length scales (Brownian regime), chemistry provides tools that allow modulating the interactions between particles upon self-assembly. However, the precise control over the size and shape of the clusters, sensitivity toward environmental factors, as well as distances between the building blocks within the clusters represent formidable challenges that may lead to the development of new strategies for the fabrication of nanoscale devices. Particularly attractive is the use of metallic nanoparticles, which exhibit tunable optical activity, rendering them promising materials for applications in fields as important as biodiagnostics[1] or energy conversion.[2]

Liquid-phase reversible assembly of gold nanoparticles into three-dimensional superstructures can be achieved by applying a variety of attractive forces. Examples of such forces are light-modulated dipole–dipole interactions between ligand molecules,[3] electrostatic interactions between oppositely charged particles,[4] or temperature-dependent hydrogen bonding between grafted DNA molecules.[5,6] Experimental control over these interactions can be provided by well-understood theoretical models that help us to predict the processes that take place in these systems.

Interestingly, solvent-mediated self-assembly of nanoparticles, which has often been intuitively associated with hydrophobic effects,[7] is still poorly understood. Hydrophobic interactions are the most important nonspecific interactions in biological systems and are responsible, for example, for the creation of lipid bilayers and determination of the conformation of proteins in water.[8] The origin of hydrophobic interactions is related to the rearrangement of water molecules as two hydrophobic species come close to each other.[9] In the context of colloid chemistry, hydrophobic interactions have helped to explain qualitatively why hydrophobic particles can gather inside oil droplets during emulsification processes, and why they form

* Address correspondence to mgrzelczak@cicbiomagune.es, llizmarzan@cicbiomagune.es.

Received for review October 15, 2012 and accepted November 27, 2012.

Published online November 28, 2012
10.1021/nn3047605

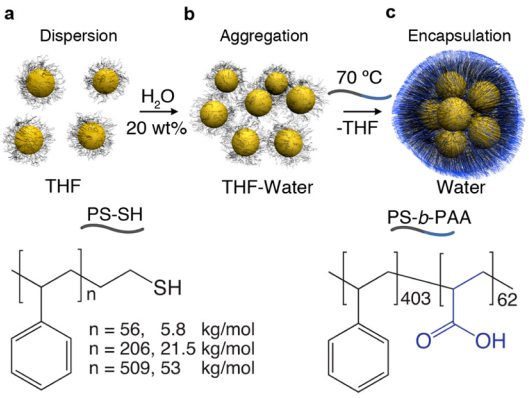

Scheme 1. Three-dimensional self-assembly of polystyrene-coated gold nanoparticles. (a) Colloidal dispersion of polystyrene coated gold nanoparticles in THF. (b) The aggregation starts upon addition of a nonsolvent (water, −20 wt %). (c) The addition of polymeric surfactant (PS-*b*-PAA) at any time during aggregation suppresses further aggregation. Mild thermal treatment leads to expelling THF and induces rearrangement of the particles inside the hydrophobic core, while the polyacrylic shell ensures stability of the clusters in water.

3D colloidal crystals upon oil evaporation.[10−14] Similarly, hydrophobic effects have been invoked to justify the solvent-mediated self-assembly of gold nanorods stabilized with hydrophobic polymers.[15,16] Besides the constantly increasing complexity of the nanoassemblies induced by hydrophobic interactions,[17−20] understanding them on the level of colloidal interactions remains a challenging task.

We show in this article that polystyrene (PS)-stabilized spherical gold nanoparticles dispersed in tetrahydrofuran (THF) can form aggregates upon the addition of water, which is a poor solvent for PS (Scheme 1a,b). We refer hereafter to such aggregates as "clusters", since control over the size and monodispersity differentiate them from the commonly accepted meaning of "aggregates" in colloid science. We derived a quantitative model that accounts for the attractive hydrophobic interactions that are responsible for the assembly process. Additionally, the growth of the clusters can be quenched by the addition of a polymeric surfactant comprising hydrophobic (polystyrene) and hydrophilic (poly(acrylic acid)) blocks (PS-*b*-PAA). While the amphiphilic nature of the polymeric surfactant allows for sequestration of clusters inside the hydrophobic core, the hydrophilic outer surface of the micelles (comprising the PAA blocks) ensures stability in polar solvents (Scheme 1c) and allows improved visualization.

RESULTS AND DISCUSSION

Geometrical features of the nanoparticle clusters, such as aggregate size and interparticle distance, were controlled by adjusting the diameter of the gold nanoparticles and the length of polystyrene chains. Since the clusters assemble by noncovalent interactions, redispersion in a good solvent induces disintegration

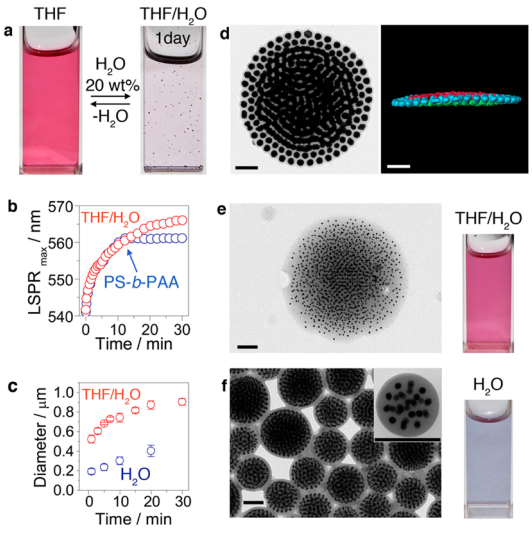

Figure 1. Formation of rigid clusters of Au nanoparticles. (a) Visible changes of the solution containing Au_{18}@PS_{509} upon aggregation by hydrophobic interactions. (b) Time trace of LSPR maxima showing a red shift upon addition of water (red dots). Addition of PS-*b*-PAA (indicated by arrow) at 10 min of aggregation time inhibits further spectral shifts. (c) Size evolution (DLS) of the clusters as a function of time (red dots). Encapsulation of the aggregates in PS-*b*-PAA and transfer to water lead to a decrease of clusters size by half (blue dots). (d−f) TEM images at different stages of the assembly process within 10 min of aggregation time. (d) Before addition of PS-*b*-PAA the clusters form flat, disk-like structures upon drying, as confirmed by 3D electron tomography reconstruction. (e) Quenching of the aggregation by the addition of PS-*b*-PAA. Encapsulation is reflected in clearly visible organic matter around the clusters, which remain colloidal stable in THF−water mixture. (f) Thermal treatment of the quenched clusters makes them rigid and stable in aqueous solutions. All scale bars correspond to 200 nm.

of the structures to release the particles back into solution.

Addition of water (20 wt %) to a THF solution containing 18.0 ± 0.5 nm gold nanoparticles (Au_{18}), stabilized with hydrophobic polystyrene chains (Au_{18}@PS_{509}), slowly induces a color change (from red to pink/violet) and finally gives rise to aggregation and subsequent precipitation (Figure 1a). The color change is reflected in the progressive redshift of the maximum of the localized surface plasmon resonance (LSPR) band—the optical fingerprint of gold particles—from 540 to 565 nm during the first 30 min after water addition (Figure 1b, red). The observed redshift is due to the progressive decrease in interparticle distances and increase in cluster size, which was confirmed by dynamic light scattering (DLS). During the first 30 min after water addition, the mean size of the clusters increased from 100 nm (hydrodynamic diameter of the dispersed Au_{18}@PS_{509} particles) up to 904 nm (Figure 1c, red). Transmission electron microscopy (TEM) from the solution at early stages of aggregation (10 min) showed quasi-flat assemblies in the form of circular islands with sizes between 1 and 3 μm (Figure 1d). We propose that, upon water addition,

the Au nanoparticles assemble into spherical clusters in solution, which collapse onto the solid substrate (carbon film) upon solvent evaporation to form flat disk-like assemblies. Keeping in mind that direct drop-casting of the particles from THF solution resulted in the formation of extended hexagonal close packed monolayers (see Supporting Information, section 1), the observation of such disk-like assemblies supports the hypothesis that the nanoparticles start interacting already in the THF/water mixture.

The aggregation of the polystyrene-coated gold nanoparticles in the THF/water mixture can be quantitatively explained by considering that the dominant attractive force is due to hydrophobic interactions. In pure THF, brush repulsion between the polymer chains of adjacent particles overcomes the attractive van der Waals (vdW) interactions.[21] However, in the presence of water, the hydrophobic polystyrene chains compress and attract each other to expel solvent molecules (water and THF) into the bulk and thereby minimize the free energy of the system. The combination of vdW,[22] brush repulsion,[21] and hydrophobic interactions[23] results in the following overall expression (see Supporting Information, section 2 for details):

$$E = \frac{200RL^2kT}{\pi s^3} e^{-\pi D/L} - \frac{R}{6}\left(\frac{A_{232}}{D-2L} - \frac{2A_{123}}{D-L} + \frac{A_{121}}{D}\right) - 4\pi RD_0\gamma(1-f)\, e^{-(D-2L)/D_0} \quad (1)$$

The first two components correspond to polymer brush and vdW interactions, where R is the radius of the nanoparticles, L is the length of the polymer chain, s is the footprint diameter of a single polymer chain, and A is the Hamaker constant ($A_{232} = A_{PS\text{-}THF\text{-}PS}$ and $A_{123} = A_{Au\text{-}PS\text{-}THF}$). The third term in eq 1 accounts for hydrophobic interactions,[23] where γ is the interfacial energy of the polystyrene in a specific solvent composition, and D_0 is the hydrophobic decay length. The hydrophobic term is effectively zero in the pure solvent case, when $f = 1$ in eq 1, and contributes an increasingly attractive hydrophobic interaction as f progressively decreases from 1 to 0. Here, f is termed the `hydrophobic−hydrophilic balance` because it can be used to generally describe the spectrum of solvent-based interactions: repulsive hydrophilic interactions for $f > 1$ (arising from steric-hydration or solvation interactions due to enhanced density of strongly adsorbed solvent molecules), and attractive hydrophobic interactions for $f < 1$ (arising from hydrophobic or solvophobic interactions due to reduced or `depleted` solvent density near an interface). Thus, we use $f = 1$ to describe the interactions in pure THF. Without further knowledge of the interfacial structure, a range of f values between 0 and 1 were used to describe the interactions in the THF/water mixture.

As shown in Figure 2, when only vdW and brush interactions are considered (pure THF solvent, $f = 1$), there is a strong energy barrier against aggregation of about $11kT$ and a positive energy minimum at a cut off distance of 1.5 Å. As the hydrophobic parameter f is decreased from 1 to 0, which progressively increases the hydrophobic contribution, the energy barrier decreases to $0.4kT$ (mixed solvent, $f = 0$). The primary minimum at polystyrene−polystyrene contact is nearly $200kT$ for the fully hydrophobic case ($f = 0$). While the exact value of f for this system remains unknown, we have shown that a reasonable range of values for f lead to a weak repulsive barrier and strong adhesion, which is in agreement with the observed experimental trends. This calculation illustrates the transition from a stable to an unstable suspension as water is added to the THF solution, clearly demonstrating that the system undergoes hydrophobic aggregation.

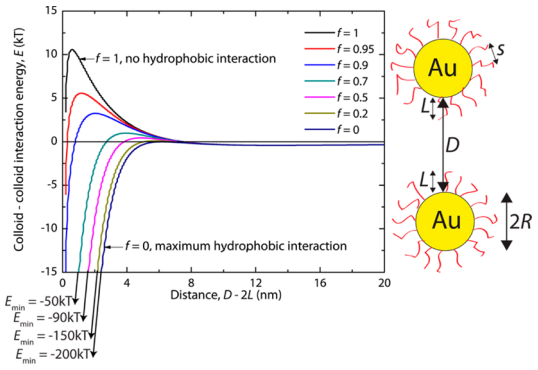

Figure 2. Effect of hydrophobic interactions on the colloidal stability of gold nanoparticles. Colloid−colloid interaction energy E as a function of interparticle separation D, calculated using eq 1 for different solvent compositions f. Length of PS chain $L = 7$ nm; footprint diameter $s = 1.4$ nm; $T = 298$ K; Hamaker constants $A_{232}=A_{PS\text{-}THF\text{-}PS} = 5.7 \times 10^{-21}$ J and $A_{123}=A_{Au\text{-}PS\text{-}THF} = 2.3 \times 10^{-20}$ J; radius of gold nanoparticles $R = 9$ nm; hydrophobic decay length $D_0 = 1$ nm; interfacial energy $\gamma = 8$ mJ/m^2.

The clusters can be stabilized by preventing uncontrolled precipitation, through the addition of a polymeric surfactant that is able to sequester the particles into the hydrophobic core of its micelles.[24−31] We used an amphiphilic diblock copolymer (polystyrene-*b*-poly(acrylic acid) , PS_{403}-*b*-PAA_{62}, see Figure 1) that forms micelles in the THF/water mixture.[32] The addition of PS_{403}-*b*-PAA_{62} (in THF) during clustering of the particles (10 min after addition of water) was found to quench aggregation and prevent further growth, as confirmed by the invariance of the LSPR band (Scheme 1b, blue dots). TEM characterization from the stabilized suspension revealed the presence of apparently spherical clusters containing the nanoparticles embedded in some organic material (Figure 1e). This morphology suggests the flexible and adaptable character of the assemblies, which arises from the presence of the solvent in the hydrophobic core. The solvent acts as a plasticizer and thus increases the exchange rate at which unassociated copolymer chains and micelles are able to reach thermodynamic equilibrium.[33] However,

for the micelles that contain nanoparticles stabilized with polystyrene, equilibrium may never be reached over reasonable time scales, as the temperature at which the clustering occurs is far below the glass transition temperature of bulk polystyrene. Indeed, the LSPR maximum was found to remain unchanged for at least 4 weeks. To further displace the system out of equilibrium we applied a thermal treatment (70 °C) that resulted in expelled solvent from the hydrophobic cores. Subsequent transfer of the clusters into pure water helps maintain a compact polystyrene core, resulting in size reduction of the clusters by approximately half the original diameter (Figure 1c, blue dots and Figure 1f). While solidification of the hydrophobic polystyrene core promotes uniform filling of the three-dimensional inner space by the nanoparticles, electrostatic interactions between the hydrophilic outer surfaces (measured zeta potential = −37.5 mV) ensure colloidal stability of the clusters in pure water. As the kinetically frozen aggregates manifest morphological stability over long periods of time (4 months), we further characterized them without additional processing.

In general, liquid-phase aggregation of the spherical particles *via* nonspecific interactions leads to formation of isotropic assemblies (Scheme 1f), whose overall dimensions reflect the magnitude of the interactions. Hydrophobic interactions, as shown in eq 1, are proportional to the interfacial energy γ, which in turn is proportional to solvent composition (water content), or, in the case of polymers, is linearly proportional to $M_n^{-2/3}$.[34] Thus, by controlling the molecular weight of the grafted polymer or the amount of water in the mixture we expect that the hydrophobic interactions can be modulated, or in geometric terms, that the size of the assemblies can be tuned. We first investigated the influence of the length of the polymer chains using Au_{18} stabilized with thiolated polystyrene of three different molecular weights: 5.8, 21.5, and 53.0 kg/mol. While keeping aggregation time constant (10 min), as well as the water content (20 wt %) and particle concentration (1×10^{-9} M), the final sizes of the clusters were established to be proportional to the length of the PS chains (Figure 3a). Additionally, this trend was found to be independent of nanoparticle diameter. For bigger particles (40.0 ± 0.9 nm, Au_{40}; and 61.7 ± 1.5 nm, $Au_{60\ nm}$) the average size of the clusters also increases with increasing length of the PS chains (Figure 3a, for full TEM characterization see Supporting Information, section 3). Similarly, modulation of polystyrene interfacial energy through solvent composition (varying H_2O content from 10 to 30 wt %) also affects cluster size, leading to a gradual increase with increasing amount of water (see Supporting Information, section 4). These trends indicate that subtle control over the interfacial energies of the stabilizing polymer *via* changes in chain length or solvent composition can determine the final size of the clusters.

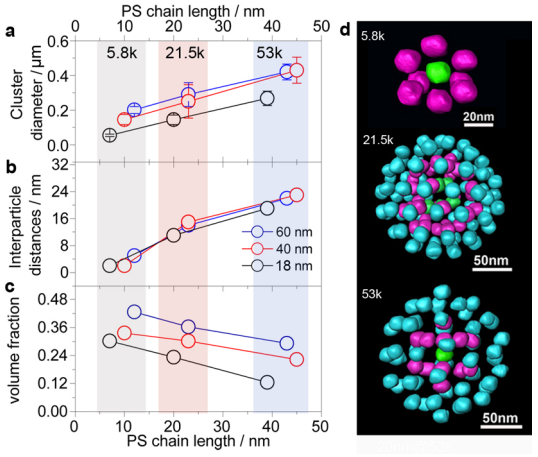

Figure 3. Control over cluster size, interparticle distance, and volume fraction. (a) Average cluster diameter as a function of length of the PS chains for 18, 40, and 60 nm gold nanoparticles. Each length corresponds to a specific molecular weight of the PS chains, as indicated by rectangular areas with different colors. (b) Average interparticle distance as a function of length of the PS chains. (c) Nanoparticles volume fraction as a function of the length of the PS chains. (d) 3D electron tomography reconstructions of clusters comprising Au_{18} with progressively increasing lengths of the PS chains. Note that interparticle distances increase with increasing PS chain length.

Finally, the presence of dissolved gas can strongly affect the magnitude of the hydrophobic interaction. Recent studies have shown that there are three regimes that can contribute to the hydrophobic interactions between micrometer-sized PS surfaces:[35] (1) a very long-range interaction regime from ∼20 nm to hundreds of nanometers, due to bridging by microscopic and submicroscopic bubbles; (2) a possible intermediate interaction regime, typically ranging from several nanometers up to 10−20 nm, due to an enhanced Hamaker constant associated with enhanced proton-hopping in water (so-called Grotthuss effect); and (3) a short-range interaction regime (from <1 nm to several nanometers), due to entropic structural effects of water close to the hydrophobic surfaces. Especially challenging has been the finding of the long-range interactions regime, as the bridging of air bubbles between the polymer surfaces depends sensitively on the experimental conditions.[35,36] Nevertheless, the presence of air upon the clustering of sub-100 nm particles can also affect the geometry of the assemblies. We found that ∼1% of our spherical assemblies present voids, suggesting that hydrophobic air bubbles are present and attract the hydrophobic particles to the interface between the air bubble and the solvent, thereby playing a structure-directing role for nucleating particle assemblies (see Supporting Information, section 5). Therefore, the long-range interaction regime upon the clustering of particles with diameters smaller than air bubbles can be excluded, indicating the predominance of the intermediate and short-range interaction regimes. Interestingly, from the

standpoint of geometrical complexity of the assemblies, the gold particles at the air bubble interface could be an alternative method for creating hollow spherical assemblies.[37]

Characterization of the Au nanoparticle clusters by electron tomography reconstructions provides insight into the spatial distribution of the particles in the cluster as well as interparticle distances. Conventional electron microscopy yields 2-dimensional projections of 3-dimensional objects, which may lead to incomplete results. Especially for assemblies such as the ones studied here, it is of great importance to investigate the 3-dimensional spatial distribution of the individual particles in a cluster. Such studies can be performed by electron tomography, a technique in which a large number of 2-dimensional electron microscopy images is combined in a 3-dimensional reconstruction. Examples illustrating the outcome of these reconstructions are presented in Figure 3. Once such a 3-dimensional reconstruction is obtained, interparticle distances can also be calculated from the electron tomography reconstruction. Analysis of these parameters showed that the particles uniformly fill the polystyrene cores, with uniform edge-to-edge distances and apparently a certain degree of order (see Supporting Information, section 6). Controlling the length of polymer chains allowed the modulation of the gap distances between the particles, which is particularly visible for 18 nm particles stabilized with progressively increasing PS chains (Figure 3d). Regardless of particle diameter (Au_{18}, Au_{40}, and Au_{60}), for the shortest polymer chain length, the distances were smaller (2−5 nm) as compared to the longest polymer chains (distances are 19−22 nm) (see Figure 3b). This renders the clusters accessible for molecular uptake and controlled release, which may have interesting biological applications. 3D electron tomography reconstructions also allowed the average number of particles per cluster to be estimated, which in more general terms can be presented in terms of volume fraction (Figure 3c). As expected, the volume fraction of metallic gold in the cluster increases with increasing particle diameter and decreasing polymer chain length. Limiting values of 0.1 and 0.4 were observed for clusters of Au_{18}@PS_{509} and Au_{60}@PS_{53} (Figure 3c).

Geometrical features, such as cluster size and volume fraction, aid understanding of the bulk optical response of the colloids. Regardless of the mean nanoparticle diameter, increasing the length of the PS chains increases the redshift of the plasmon band, accompanied by a significant reduction and broadening of the extinction (Figure 4a). Recent studies on DNA-induced nanoparticle clustering have shown that both increased aggregate size and volume fraction (interparticle distances) can lead to LSPR redshifts.[38] In our case, the observed redshifts are due to increasing cluster sizes, with decreasing volume fractions

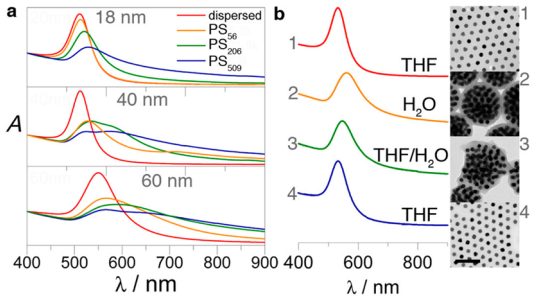

Figure 4. Optical properties and solvent-induced cluster disassembly. (a) UV−vis−NIR spectra of the clusters in water. The final position of the LSPR band is more red-shifted for longer PS chains. For Au_{40}@PS_{509} and Au_{60}@PS_{509} a second band appears that may correspond to coupled plasmon modes. (b) Reversible particle clustering in different mixture compositions and their effect on the optical response: (1) stable colloid solution of Au_{18}@PS_{509} in THF; (2) self-assembly, thermal treatment, and transfer into water maximize the redshift of the plasmon band; (3) gradual disassembly of the clusters by addition of good solvent—plasmon band blueshifts; (4) recovery of the initial plasmon band position and colloidal stability of the building blocks in a good solvent (THF).

(Figure 3a,c). With increasing cluster size, the total number of "coupled" particles contributing to the overall optical response increases. Therefore, the plasmon shift originates from the collective interactions of particles with light. This feature brings new insights into the field of plasmon engineering, indicating that the plasmonic optical window can be easily tuned independently of the available space between the particles.

As the Au nanoparticle clusters are held together by noncovalent interactions, their sensitivity to solvent composition can be expressed in terms of cyclic assembly and disassembly. Figure 4b is an example of such a process. Initially stable Au nanoparticles in organic solvent (1) are assembled into spherical clusters upon water addition and subsequently encapsulated within polymeric micelles. The amphiphilic character of the capsules ensures stability of the clusters in water (2). Addition of THF (1:1 vol) to the aqueous solution of the clusters partially solubilizes the hydrophobic polystyrene cores, leading to gradual disintegration of the assemblies (3). Removal of water by centrifugation allows recovery of the initial colloidal stability of the particles in the organic solvent (4). Each step of the reversible particle aggregation is characterized by a specific optical response, making the process easy to control.

CONCLUSIONS

We showed a new methodology for the preparation of clusters containing gold nanoparticles. Control over cluster size, interparticle distance, and overall optical response make these structures promising candidates for drug delivery, especially if release of internal cargo is required. Note, that the copolymer used here is a model system that can be replaced by conducting

or biodegradable copolymers that will bring new solutions for problems in biosensing or energy conversion. Apart from the applications, our system raises intriguing questions regarding fundamental concepts, for example in plasmon hybridization, which has still been poorly investigated for multiparticle 3D clusters.

EXPERIMENTAL SECTION

Synthesis of Gold Nanospheres (10 nm). First, gold seeds (~1.5 nm) were prepared by borohydride (10 mM, 0.3 mL) reduction of $HAuCl_4$ (0.25 mM, 5 mL) in aqueous cetyltrimethylammonium bromide solution (CTAB, 100 mM). After 30 min, an aliquot of seed solution (0.6 mL) was added to a growth solution (100 mL) containing cetyltrimethylammonium chloride (CTAC, 100 mM), $HAuCl_4$ (0.18 mM), and ascorbic acid (0.36 mM). The mixture was left undisturbed for 12 h at 25 °C. Upon synthesis, the solution was centrifuged (9000 rpm, 2h) to remove excess CTAC and ascorbic acid, and redispersed in water to a final gold concentration equal to 2.5 mM.

Synthesis of Gold Nanospheres (18, 40, and 60 nm). To grow 10 nm gold nanospheres up to 18, 40, and 60 nm diameter, a volume of gold seed solution 2.5 mM (0.71, 0.08, or 0.02 mL) was added under magnetic stirring to a growth solution (25 mL) containing benzyldimethylammonium chloride (BDAC, 100 mM), $HAuCl_4$ (0.5 mM), and ascorbic acid (1 mM). The mixture was left undisturbed for 30 min at 30 °C, and then washed twice by centrifugation. The particles were finally dispersed in water to a final gold concentration equal to 5 mM.

Ligand Exchange. To replace surfactant with hydrophobic polymer, thiolated polystyrene (Polymer Source, Inc.) with different molecular weights (5.8, 21.5, and 53 kg/mol) were used. The solution of gold nanoparticles of desired diameter (5 mM, 1 mL) was added dropwise under sonication to a THF solution (10 mL) of PS-SH (1 molecule of PS-SH per nm^2 of gold surface). The solution was left for 15 min in an ultrasonic bath. To ensure ligand exchange, the resulting mixture was left undisturbed for 12 h, and then centrifuged twice (7000 rpm, 60 min). The particles were finally dispersed in THF to a final gold concentration equal to 2.5 mM.

Self-Assembly and Polymer Encapsulation. In a typical self-assembly experiment, water (0.4 mL) was added to the Au@PS colloid (1.6 mL, THF) under magnetic stirring. In the final mixture the concentration of gold was 0.25 mM. The solution was left undisturbed for 10 min under ambient condition. To quench further aggregation, a solution of PS_{403}-*b*-PAA_{62} in THF (6 mg/mL, 0.2 mL) was added. Subsequently, the water content was increased up to 35 wt %, followed by increasing the temperature up to 70 °C, which was maintained for 1 h. The final solution was centrifuged twice (3500 rpm, 20 min) and dispersed in pure water.

Three-Dimensional Electron Tomography Reconstructions. TEM specimens were prepared by applying drops of solution onto a carbon-coated TEM copper grid. A series of high angle annular dark field-scanning transmission electron microscopy (HAADF-STEM) images was acquired with 2° tilt increments using a Tecnai G2 transmission electron microscope operated at 200 kV and a Fischione 2020 single tilt holder. Three-dimensional (3D) reconstruction of the clusters was carried out using the simultaneously iterative reconstruction technique[39] and by the total variation minimization reconstruction technique.[40]

Conflict of Interest: The authors declare no competing financial interest.

Acknowledgment. Dedicated to Mariano Sánchez, *in memoriam*. This work was supported by the Spanish MINECO under Grant No. MAT2010-15374, the ERC Advanced Grant PLASMAQUO (267867), the ERC Advanced Grant COUNTATOMS (24691), the EU Grant No. FP7-INFRASTRUCT-2010-1, 262348 (ESMI) and the U.S. National Science Foundation under Grant No. CHE-1059108. M.G. acknowledges receipt of a Juan de la Cierva Fellowship from the Spanish MINECO and IKERBASQUE Basque foundation for Science.

Supporting Information Available: TEM images of extended monolayers of Au@PS; theoretical modeling of hydrophobic interactions; data showing control over cluster size and interparticle gap distance; effects of water on cluster size and of bubbles on cluster morphology. This material is available free of charge *via* the Internet at http://pubs.acs.org.

REFERENCES AND NOTES

1. Rosi, N. L.; Mirkin, C. A. Nanostructures in Biodiagnostics. *Chem. Rev.* **2005**, *105*, 1547–1562.
2. Linic, S.; Christopher, P.; Ingram, D. B. Plasmonic-Metal Nanostructures for Efficient Conversion of Solar to Chemical Energy. *Nat. Mater.* **2011**, *10*, 911–921.
3. Klajn, R.; Bishop, K. J. M.; Grzybowski, B. A. Light-Controlled Self-Assembly of Reversible and Irreversible Nanoparticle Suprastructures. *Proc. Natl. Acad. Sci.* **2007**, *104*, 10305–10309.
4. Kalsin, A. M.; Fialkowski, M.; Paszewski, M.; Smoukov, S. K.; Bishop, K. J. M.; Grzybowski, B. A. Electrostatic Self-Assembly of Binary Nanoparticle Crystals with a Diamond-like Lattice. *Science* **2006**, *312*, 420–424.
5. Nykypanchuk, D.; Maye, M. M.; Lelie, D.; van der; Gang, O. DNA-Guided Crystallization of Colloidal Nanoparticles. *Nature* **2008**, *451*, 549–552.
6. Park, S. Y.; Lytton-Jean, A. K. R.; Lee, B.; Weigand, S.; Schatz, G. C.; Mirkin, C. A. DNA-Programmable Nanoparticle Crystallization. *Nature* **2008**, *451*, 553–556.
7. Tanford, C. The Hydrophobic Effect and the Organization of Living Matter. *Science* **1978**, *200*, 1012–1018.
8. Hammer, M. U.; Anderson, T. H.; Chaimovich, A.; Shell, M. S.; Israelachvili, J. The Search for the Hydrophobic Force Law. *Faraday Discuss.* **2010**, *146*, 299.
9. Israelachvili, J.; Pashley, R. The Hydrophobic Interaction Is Long Range, Decaying Exponentially with Distance. *Nature* **1982**, *300*, 341–342.
10. Bai, F.; Wang, D.; Huo, Z.; Chen, W.; Liu, L.; Liang, X.; Chen, C.; Wang, X.; Peng, Q.; Li, Y. A Versatile Bottom-up Assembly Approach to Colloidal Spheres from Nanocrystals. *Angew. Chem., Int. Ed.* **2007**, *46*, 6650–6653.
11. Kim, J.; Lee, J. E.; Lee, S. H.; Yu, J. H.; Lee, J. H.; Park, T. G.; Hyeon, T. Designed Fabrication of a Multifunctional Polymer Nanomedical Platform for Simultaneous Cancer-Targeted Imaging and Magnetically Guided Drug Delivery. *Adv. Mater.* **2008**, *20*, 478–483.
12. Zhuang, J.; Wu, H.; Yang, Y.; Cao, Y. C. Supercrystalline Colloidal Particles from Artificial Atoms. *J. Am. Chem. Soc.* **2007**, *129*, 14166–14167.
13. Lacava, J.; Born, P.; Kraus, T. Nanoparticle Clusters with Lennard-Jones Geometries. *Nano Lett.* **2012**, *12*, 3279–3282.
14. Qiu, P.; Jensen, C.; Charity, N.; Towner, R.; Mao, C. Oil Phase Evaporation-Induced Self-Assembly of Hydrophobic Nanoparticles into Spherical Clusters with Controlled Surface Chemistry in an Oil-in-Water Dispersion and Comparison of Behaviors of Individual and Clustered Iron Oxide Nanoparticles. *J. Am. Chem. Soc.* **2010**, *132*, 17724–17732.
15. Nie, Z.; Fava, D.; Kumacheva, E.; Zou, S.; Walker, G. C.; Rubinstein, M. Self-Assembly of Metal–Polymer Analogues of Amphiphilic Triblock Copolymers. *Nat. Mater.* **2007**, *6*, 609–614.
16. Nie, Z.; Fava, D.; Rubinstein, M.; Kumacheva, E. Supramolecular" Assembly of Gold Nanorods End-Terminated with Polymer "Pom-Poms": Effect of Pom-Pom Structure on the Association Modes. *J. Am. Chem. Soc.* **2008**, *130*, 3683–3689.
17. Wang, Y.; Chen, G.; Yang, M.; Silber, G.; Xing, S.; Tan, L. H.; Wang, F.; Feng, Y.; Liu, X.; Li, S.; *et al*. A Systems Approach

Towards the Stoichiometry-Controlled Hetero-assembly of Nanoparticles. *Nat. Commun.* **2010**, *1*, 87.
18. Xu, J.; Wang, H.; Liu, C.; Yang, Y.; Chen, T.; Wang, Y.; Wang, F.; Liu, X.; Xing, B.; Chen, H. Mechanical Nanosprings: Induced Coiling and Uncoiling of Ultrathin Au Nanowires. *J. Am. Chem. Soc.* **2010**, *132*, 11920–11922.
19. Wang, H.; Chen, L.; Shen, X.; Zhu, L.; He, J.; Chen, H. Unconventional Chain-Growth Mode in the Assembly of Colloidal Gold Nanoparticles. *Angew. Chem., Int. Ed.* **2012**, *51*, 8021–8025.
20. Grzelczak, M.; Sánchez-Iglesias, A.; Mezerji, H. H.; Bals, S.; Pérez-Juste, J.; Liz-Marzan, L. M. Steric Hindrance Induces Crosslike Self-Assembly of Gold Nanodumbbells. *Nano Lett.* **2012**, *12*, 4380–4384.
21. Yockell-Lelièvre, H.; Desbiens, J.; Ritcey, A. M. Two-Dimensional Self-Organization of Polystyrene-Capped Gold Nanoparticles. *Langmuir* **2007**, *23*, 2843–2850.
22. Israelachvili, J. N. *Intermolecular and Surface Forces,* 3rd ed.; Academic Press: San Diego, CA, 2010.
23. Donaldson, S. H., Jr; Lee, C. T.; Chmelka, B. F.; Israelachvili, J. N. General Hydrophobic Interaction Potential for Surfactant/lipid Bilayers from Direct Force Measurements Between Light-modulated Bilayers. *Proc. Natl. Acad. Sci. U.S.A.* **2011**, *108*, 15699–15704.
24. Euliss, L. E.; Grancharov, S. G.; O'Brien, S.; Deming, T. J.; Stucky, G. D.; Murray, C. B.; Held, G. A. Cooperative Assembly of Magnetic Nanoparticles and Block Copolypeptides in Aqueous Media. *Nano Lett.* **2003**, *3*, 1489–1493.
25. Kim, B.-S.; Qiu, J.-M.; Wang, J.-P.; Taton, T. A. Magnetomicelles: Composite Nanostructures from Magnetic Nanoparticles and Cross-Linked Amphiphilic Block Copolymers. *Nano Lett.* **2005**, *5*, 1987–1991.
26. Yusuf, H.; Kim, W.-G.; Lee, D. H.; Guo, Y.; Moffitt, M. G. Size Control of Mesoscale Aqueous Assemblies of Quantum Dots and Block Copolymers. *Langmuir* **2006**, *23*, 868–878.
27. Sanchez-Gaytan, B. L.; Cui, W.; Kim, Y.; Mendez-Polanco, M. A.; Duncan, T. V.; Fryd, M.; Wayland, B. B.; Park, S.-J. Interfacial Assembly of Nanoparticles in Discrete Block-Copolymer Aggregates. *Angew. Chem., Int. Ed.* **2007**, *46*, 9235–9238.
28. Kim, B.-S.; Taton, T. A. Multicomponent Nanoparticles *via* Self-Assembly with Cross-Linked Block Copolymer Surfactants. *Langmuir* **2006**, *23*, 2198–2202.
29. Wang, X.; Li, G.; Chen, T.; Yang, M.; Zhang, Z.; Wu, T.; Chen, H. Polymer-Encapsulated Gold-Nanoparticle Dimers: Facile Preparation and Catalytical Application in Guided Growth of Dimeric ZnO-Nanowires. *Nano Lett.* **2008**, *8*, 2643–2647.
30. Poeselt, E.; Fischer, S.; Foerster, S.; Weller, H. Highly Stable Biocompatible Inorganic Nanoparticles by Self-Assembly of Triblock-Copolymer Ligands. *Langmuir* **2009**, *25*, 13906–13913.
31. Mai, Y.; Eisenberg, A. Controlled Incorporation of Particles into the Central Portion of Block Copolymer Rods and Micelles. *Macromolecules* **2011**, *44*, 3179–3183.
32. Zhang, L.; Eisenberg, A. Multiple Morphologies of "Crew-Cut" Aggregates of Polystyrene-*b*-poly(acrylic acid) Block Copolymers. *Science* **1995**, *268*, 1728–1731.
33. Luo, L.; Eisenberg, A. Thermodynamic Size Control of Block Copolymer Vesicles in Solution. *Langmuir* **2001**, *17*, 6804–6811.
34. Wu, S. *Polymer Interface and Adhesion*, 1st ed.; CRC Press: Boca Raton, FL, 1982.
35. Faghihnejad, A.; Zeng, H. Hydrophobic Interactions Between Polymer Surfaces: Using Polystyrene as a Model System. *Soft Matter* **2012**, *8*, 2746.
36. Meyer, E. E.; Rosenberg, K. J.; Israelachvili, J. Recent Progress in Understanding Hydrophobic Interactions. *Proc. Natl. Acad. Sci. U.S.A.* **2006**, *103*, 15739–15746.
37. He, J.; Liu, Y.; Babu, T.; Wei, Z.; Nie, Z. Self-Assembly of Inorganic Nanoparticle Vesicles and Tubules Driven by Tethered Linear Block Copolymers. *J. Am. Chem. Soc.* **2012**, *134*, 11342–11345.
38. Storhoff, J. J.; Lazarides, A. A.; Mucic, R. C.; Mirkin, C. A.; Letsinger, R. L.; Schatz, G. C. What Controls the Optical Properties of DNA-Linked Gold Nanoparticle Assemblies? *J. Am. Chem. Soc.* **2000**, *122*, 4640–4650.
39. Gordon, R.; Bender, R.; Herman, G. T. Algebraic Reconstruction Techniques (ART) for Three-Dimensional Electron Microscopy and X-ray Photography. *J. Theor. Biol.* **1970**, *29*, 471–481.
40. Goris, B.; Broek, W.; Van den; Batenburg, K. J.; Heidari Mezerji, H.; Bals, S. Electron Tomography Based on a Total Variation Minimization Reconstruction Technique. *Ultramicroscopy* **2012**, *113*, 120–130.